journal

Reprinted from the Journal of the American Ceramic Society, Vol. 73, No. 8, August 1990

J. Am. Ceram. Soc., 73 [8] 2419–27 (1990)

Role of Grain Size in the Strength and *R*-Curve Properties of Alumina

Prapaipan Chantikul,† Stephen J. Bennison,*,‡ and Brian R. Lawn*

Ceramics Division, National Institute of Standards and Technology, Gaithersburg, Maryland 20899

An investigation of the interrelationships between strength, crack-resistance (*R*-curve) characteristics, and grain size for alumina ceramics has been carried out. Results of indentation–strength measurements on high-density aluminas with uniform grain structures in the size range 2 to 80 μm are presented. A theoretical fit to the data, obtained by adjusting parameters of a constitutive frictional-pullout relation in a grain-bridging model, allows determination of the critical microstructural parameters controlling the *R*-curve behavior of these aluminas. The primary role of grain size in the toughness characteristic is to determine the scale of grain pullout at the bridged interface. It is shown that the strength properties are a complex function of the bridged microstructure, governed at all but the finest grain sizes by the stabilizing effect of the *R*-curve. The analysis confirms the usual negative dependence of strength on grain size for natural flaws that are small relative to the grain size, but the dependence does not conform exactly to the −½ power predicted on the basis of classical "Griffith–Orowan" flaws. The analysis provides a self-consistent account of the well-documented transition from "Orowan" to "Petch" behavior. [Key words: grain size, strength, *R*-curve, alumina, bridging.]

I. Introduction

THE influence of grain size on the strength of intrinsically brittle solids, particularly of aluminas and other noncubic ceramics, has been well documented.[1–14] Generally, the strength is observed to decline with coarsening of the grain structure. An understanding of the strength/grain-size dependence is an important element in the microstructural design of structural ceramics.

The earliest nonempirical accounts of the observed trends[9] were based on the simplistic Griffith concept of spontaneous failure from a dominant flaw. If it is assumed that the intrinsic flaw scales with grain size and that the toughness is single-valued, a so-called "Orowan" relation ensues in which the strength is proportional to the inverse square root of grain size.[15] Most data can be force-fitted reasonably well with this relation down to "intermediate" grain sizes (10 to 40 μm in alumina), at which point the size dependence is markedly reduced.[9,10] This latter region is manifested as a secondary, "Petch" branch of low slope and nonzero intercept on a strength versus (grain size)$^{-1/2}$ diagram.[16] Various interpretations of the transition have been proposed: a precursor "microplasticity" stage in crack initiation from the flaw[9,10] (from literal adaptations of the original metals-based Hall–Petch model); the stabilizing influence of local (machining, thermal expansion mismatch) residual stresses in the flaw extension[10,17]; the dominance of extrinsic (e.g., machining) flaws in the small-grain-size region,[10,12] with any microstructural dependence attributable to a monocrystal-to-polycrystal increase in the crack resistance.[10,17,18] A common feature of these proposals is that the supporting evidence cited is invariably circumstantial: i.e., the evolution of the critical flaw to final instability is never observed directly. Indeed, there is a persistent school of thought that dismisses all of the above explanations, suggesting instead that (with proper attention to distributions in grain size) the fine-grain region can be represented adequately by an Orowan relation with simple grain-size-independent, extrinsic flaw cutoff.[14]

Central to the continuing debate are the issues of nonunique toughness and crack stability. In the early 1980s efforts were made to construct broad-based models which took into account both these factors.[20–22] Those models used empirical functions to represent a monocrystal–polycrystal transition in toughness and thereby predicted a stable region of crack growth prior to failure. Again, little or no attempt was made to confirm the models with direct experimental observations of flaw micromechanics. The lack of definitive experiments on materials with well-characterized toughness/crack-size properties and properly controlled flaws has not helped to resolve the debate.[14,19,23]

More recently, direct evidence for departures from single-valued toughness in polycrystalline ceramics, predominantly in aluminas[24–29] but also in other (noncubic) materials, has become available. (Typically, for an alumina of grain size ≈20 μm, the toughness increases from a value of ≈2 to 6 MPa · m$^{1/2}$ over a crack extension ≈5 mm.) This rising toughness, termed "*R*-curve" (or "*T*-curve") behavior, becomes more pronounced as the grain size increases.[26,27] Further studies using controlled indentation flaws in alumina[30–35] demonstrate that the *R*-curve strongly stabilizes crack growth, such that the critical flaw may extend several times its original dimension prior to failure.[31] In situ observations of the indentation flaws (as well as of other well-defined crack geometries) during applied loading unequivocally identify the underlying cause of this stabilization as crack-interface bridging by interlocked grains behind the crack tip.[31,34] These same observations reveal that the crack first propagates through one or two grain diameters and then arrests ("pop-in"), and thereafter grows erratically during the prefailure growth.[31] The failure condition shows strong departures from Griffith behavior, with a pronounced tendency for the strength to become independent of indentation load in the small-flaw domain ("flaw tolerance").[30,33,35,36]

Theoretical fracture mechanics treatments of the crack-bridging process have been developed on the basis of frictional grain pullout.[32,33,36] The most recent analysis[36] makes a special effort to incorporate essential elements of the microstructure into the fundamental constitutive relation for the pullout, especially the role of thermal expansion anisotropy

R. Cook—contributing editor

Manuscript No. 197864. Received December 21, 1989; approved May 2, 1990.

Presented at the 92nd annual Meeting of the American Ceramic Society, Dallas, TX, April, 1990.

Supported by a grant from the U.S. Air Force Office of Scientific Research.

*Member, American Ceramic Society.

†Guest Scientist, on leave from the Physics Department, Faculty of Science, Chulalongkorn University, Bangkok, Thailand BKK10330.

‡Guest Scientist, on leave from the Department of Materials Science and Engineering, Lehigh University, Bethlehem, PA 18015.

stresses in augmenting grain-boundary friction. The model is thereby able to account for the observed tendency to more pronounced *R*-curves with coarsening microstructure. More appropriately, it has the necessary ingredients for a universal characterization of the grain-size dependence of strength, over a broad spectrum of flaw sizes (subgrain to multigrain) and types ("natural" as well as indentation).[36] Interestingly, the predicted dependence for natural flaws in the coarse-grained region can be significantly less than the power $-\frac{1}{2}$ of Griffith–Orowan. A preliminary comparison with some literature data on alumina appeared to substantiate this predicted departure from ideal behavior.[36]

In the present study we investigate the interrelationship between strength and grain size in greater depth. Indentation–strength experiments are conducted on high-density aluminas with uniform grain structures in the size range 2 to 80 μm. The surfaces of the specimens are finely polished to minimize the intrusion of extrinsic flaws. It is confirmed that strength is a multiregion function of grain size, governed at all but the finest microstructures ($\lesssim 5$ μm in our alumina) by the stabilizing effect of the *R*-curve. Analysis of the data in terms of the grain-bridging model provides a self-consistent account of the strength properties. For very small flaws the negative grain-size dependence of strength indeed differs (if only slightly) from power $-\frac{1}{2}$; for very large flaws the dependence is the same in the coarse-grain region, somewhat lower but still negative in the intermediate-grain region, and is actually predicted to become slightly positive in the fine-grain region. A fit of the grain-bridging model to the data, obtained by adjusting microstructural quantities in the constitutive frictional pullout law, allows deconvolution of the critical *R*-curve parameters for the alumina.

II. Experimental Procedure

(1) Preparation of Alumina Specimens

A fabrication procedure based on the Lucalox[§] process[37,38] was used to produce high-density, single-phase α-Al_2O_3 specimens with homogeneous, equiaxed grain structures. Powder preparation was carried out in class A-100 clean-room conditions. Ultra-high-purity Al_2O_3 powder[¶] was doped with trace MgO (Mg/Al = 500 at. ppm, i.e., below the solid solubility limit for Mg in Al_2O_3 at the firing temperatures used below)[39] by addition of a magnesium nitrate solution in methanol. The slurry was continuously stirred during drying and then deagglomerated by crushing. Disks 25 mm in diameter and 5 mm in thickness were fabricated by uniaxial pressing at 50 MPa using a high-purity graphite die, punch, and spacer assembly. Removal of any textural defects associated with nonhydrostatic pressures was achieved by subsequent wet-bag isostatic pressing at 350 MPa. A green density $\approx$55% of the theoretical limit was attained by this procedure.

The green disks were packed in loose powder of identical composition in high-purity alumina crucibles for heat treatment. Two firing stages were employed. The first consisted of calcining at 1150°C in air for 24 h followed by sintering at 1550°C for 30 min ($MoSi_2$ resistance furnace). This yielded specimens of $\geq$99% density with 1.8-μm grain size. The second stage involved postsintering heat treatments under reducing conditions (N_2 gas, graphite-element furnace), in separate batches at prescribed hold times and at temperatures between 1550° and 1800°C. This promoted grain growth, producing specimens in the grain-size range 2 to 80 μm. All heating cycles were carried out at a maximum heating/cooling rate of 500°C/h.

Sample specimens from each batch were subjected to microstructural characterization. Densities were measured by the Archimedes method using water as the immersion medium.[40] Surfaces were prepared for optical microscopy by diamond polishing to 1 μm. The microstructures were revealed by thermal etching (air, 1550°C, 12 min) and the grain diameters measured using the linear intercept technique.[41] Unetched specimens were examined in transmitted light for the incidence of spontaneous microcracking.

(2) Indentation–Strength Testing

Prior to testing, each remaining disk was machined to a thickness of 2.5 mm and the prospective tensile face diamond-polished to a 1-μm finish. Most specimens were indented at their face centers with a Vickers diamond pyramid at contact loads between 0.2 and 200 N. Some were left unindented as controls. All indentations were made in laboratory ambient and allowed to stand for 10 min. Biaxial strength tests were then made using a flat circular punch (4-mm diameter) on a three-point support (15-mm diameter).[42] A drop of silicone oil was placed onto the indentations prior to testing, and failure times were kept below 20 ms, to minimize effects from moisture-assisted kinetic crack growth. "Inert" strengths were calculated from the breaking loads and specimen dimensions using thin-plate formulas.[42] Special care was taken to examine all specimens after failure in the optical microscope to verify the contact site as the origin of failure. Breaks that did not pass through the indentations were incorporated into the data pool for unindented controls.

Optical and scanning electron microscopy was also used to examine the fracture surfaces to determine the relative amounts of intergranular and transgranular cracking.

III. Experimental Results

(1) Characterization of Microstructure and Fracture Surfaces

Figure 1 shows representative microstructures of two aluminas, at opposite extremes of grain size. The grain structures are equiaxed and of narrow size distribution (maximum diameter < twice mean diameter—"Hillert's criterion"[43]), as is appropriate to an investigation of a size effect. Such equiaxed structures may be taken as circumstantial evidence for the lack of any intergranular glassy phases.[44] The defect population in Fig. 1 appears to consist predominantly of surface-intersected pores at triple-point junctions (seen to better advantage in Fig. 1(B)) and occasional grain pullouts due to polishing (e.g., at upper right in Fig. 1(A)). The small scale of the defects indicates that we have attained high density: actual measurements yield $\geq$99% of theoretical density at all grain sizes.

The translucence of our materials also allowed the internal flaw population to be investigated in the bulk material, using transmitted light. Figure 2 is an example. Small pores are again evident on a substantial fraction of the triple-point sites. Such pores can be effective sources of grain-facet cracking and are thereby believed to constitute a principal component of the intrinsic flaw population in our materials. More apparent are extended microcracks, on the order of two to three grain-facet dimensions, which have generated spontaneously under the action of local thermal expansion anisotropy stresses during the processing. The first incidence of such microcracks was observed at grain sizes as low as 35 μm, beyond which the number density increased markedly with coarsening of the microstructure.

Figure 3 shows fracture surfaces of the same aluminas in Fig. 1, after biaxial strength testing. These micrographs reveal a mixture of fracture modes, $\approx$70% intergranular and $\approx$30% transgranular in our aluminas. This represents a somewhat larger proportion of transgranular mode than noted in our previous studies using a commercial alumina, which was characterized by a distinctly less uniform grain structure.[30,31]

[§]Polymers Product Division, General Electric Co., Pittsfield, MA.
[¶]AKP-HP grade (99.995% pure, 0.5-μm crystallites), Sumitomo Chemical America, New York.

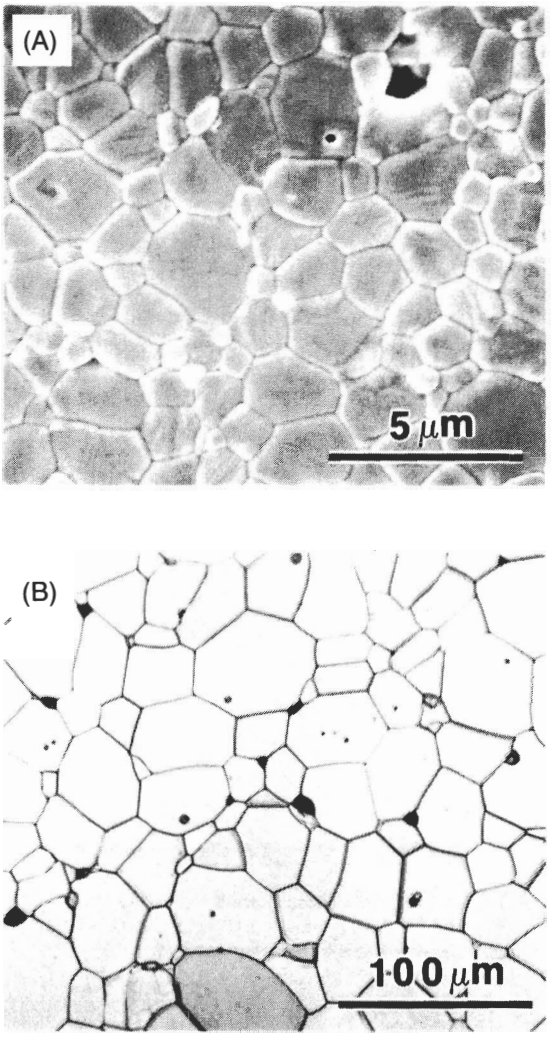

Fig. 1. Microstructure of polished alumina surfaces: (A) SEM, $\ell = 2.5$ μm; (B) optical, reflected light, $\ell = 79.8$ μm. Surfaces have been thermally etched to reveal grain structure.

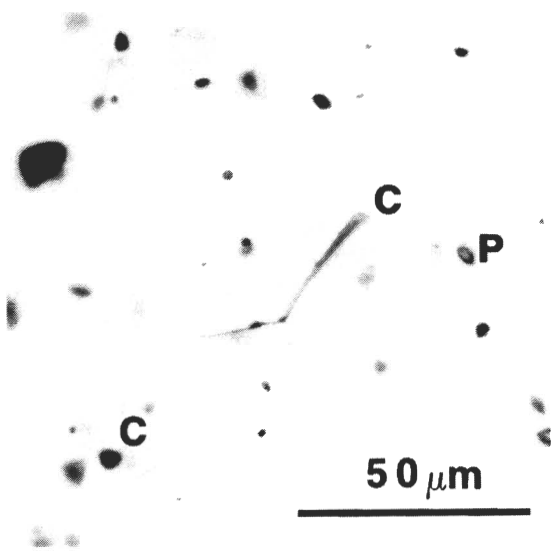

Fig. 2. Optical micrograph of alumina of grain size $\ell = 35$ μm, transmitted light. Note the triple-point pores (P) and extended microcracks (C–C).

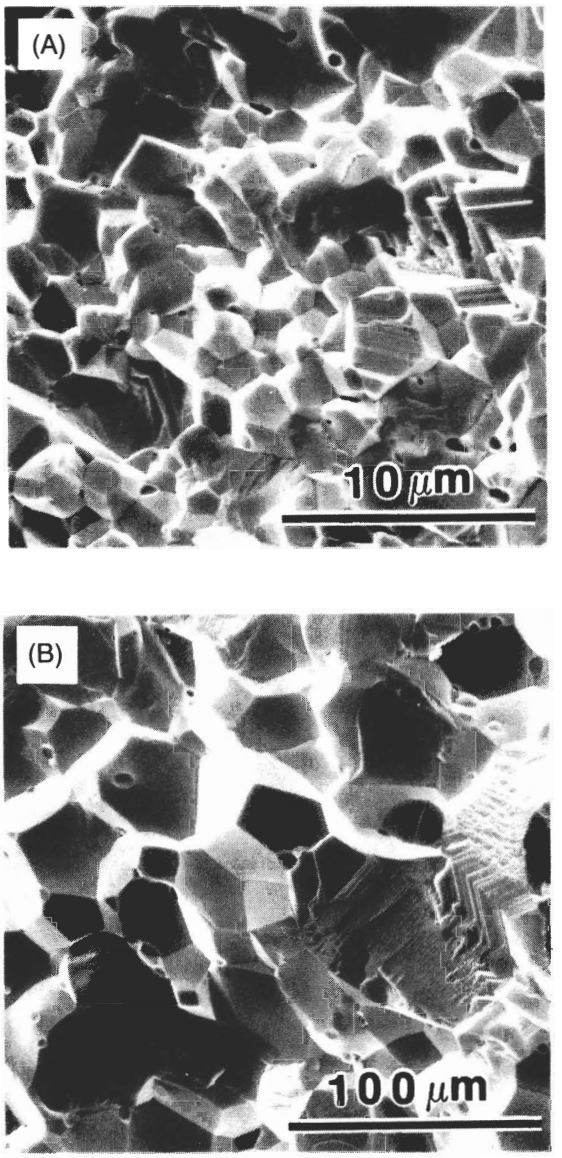

Fig. 3. Scanning electron micrographs of alumina fracture surfaces, grain sizes (A) $\ell = 2.5$ and (B) $\ell = 79.8$ μm (same specimens as Fig. 1).

Again, we may note the presence of pores at the grain-boundary junctions in Fig. 3.

(2) Indentation–Strength Data

Figure 4 plots the measured inert strengths as a function of indentation load for each grain size. Each data point represents the mean and standard deviation of an average four indentation-flaw failures; the hatched region at left represents failures from natural flaws. The solid curves through the data are best-fit predictions from the theoretical model, to be described below (Sections IV and V).

The strength data in the individual plots are marked by a distinctive tendency to a plateau at smaller indentation loads.[††] This tendency is a manifestation of the *R*-curve:[30,33,35,36] for materials with single-valued toughness, the strength should follow a simple power-law (load)$^{-1/3}$ dependence.[45–47] The

[††]Note that the plateaus in Fig. 4 are asymptotic to the strength levels for natural flaws (hatched regions at left), for all but the finest grain size, i.e., $\ell = 2.5$ μm (Fig. 4(A)). Such gradual, asymptotic transitions are a definitive characteristic of *R*-curve behavior.[30] The more abrupt, nonasymptotic cutoff in Fig. 4(A) is indicative of the dominance of extrinsic flaws. We return to this point in the Discussion.

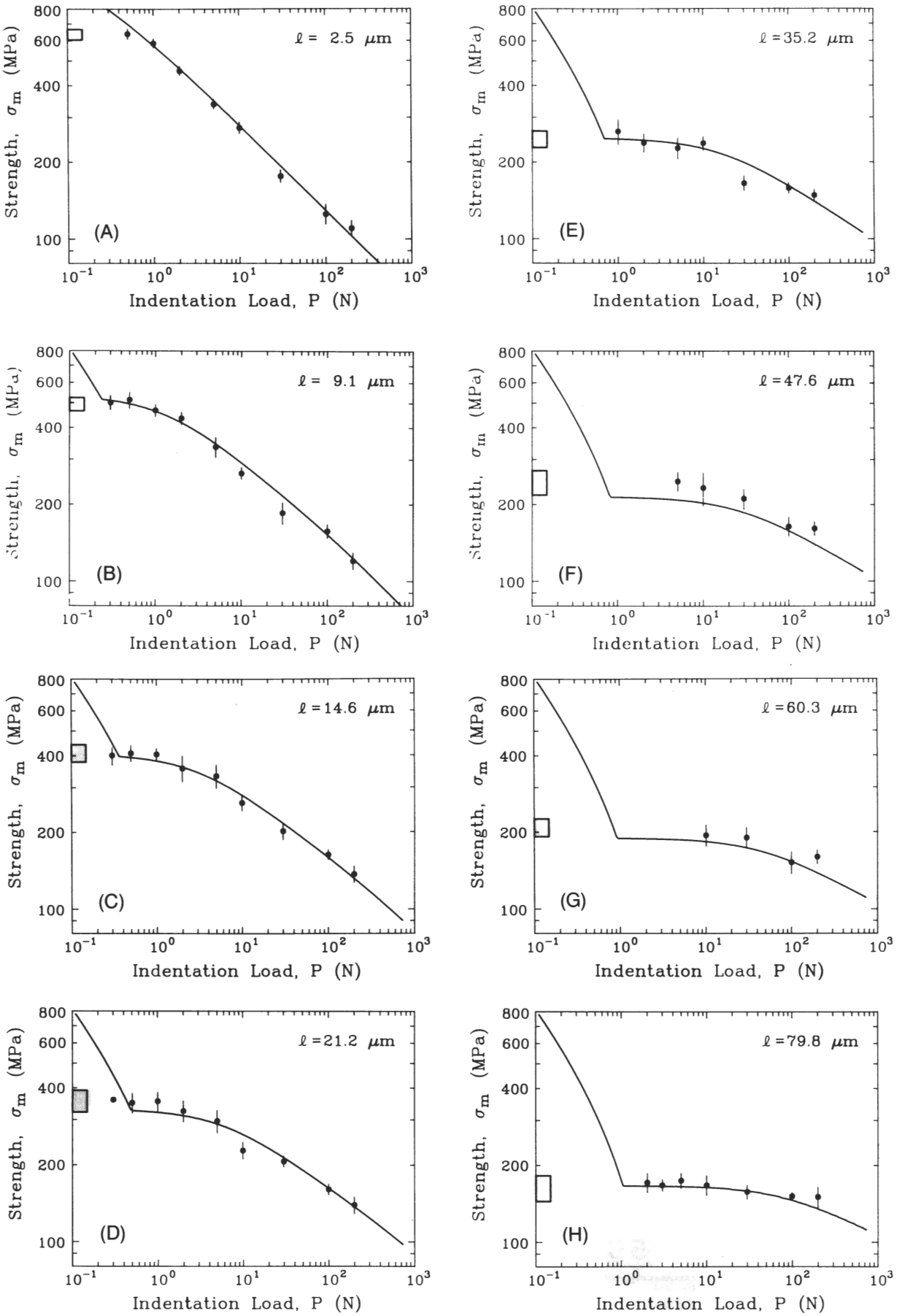

Fig. 4. Plots of inert strength σ_m, versus indentation load P, for aluminas of grain size (A) ℓ = 2.5 μm, (B) ℓ = 9.1 μm, (C) ℓ = 14.6 μm, (D) ℓ = 21.2 μm, (E) ℓ = 35.2 μm, (F) ℓ = 47.6 μm, (G) ℓ = 60.3 μm, and (H) ℓ = 79.8 μm. Curves are best fit from bridging model in Sections IV and V.

strength plateau is lower, but stronger (i.e., persists over a greater range of contact load), at larger grain sizes. One may also note a disposition for the data sets at any two grain sizes to cross each other at some point along the load axis. We shall discuss these trends in relation to transitions from Orowan to Petch behavior in Section V.

IV. Theory

We summarize here the essence of the grain-bridging theory of *R*-curve (*T*-curve) and strength characteristics in monophase ceramics as it pertains to grain size.[36] It is implicit in this endeavor that the principle of similitude applies to our materials, i.e., that the microstructure scales geometrically with grain size.

(1) Grain-Bridging and T-Curve (R-Curve)

Begin by defining a *general* stress intensity factor condition for the equilibrium of a crack subject to an applied tensile loading field, $K_a(c)$, a flaw-localized residual nucleation field, $K_r(c)$, and a microstructure-associated field, $K_\mu(c)$.[32,48,49] Equilibrium obtains when the net crack-tip field, $K_*(c)$, just balances the toughness associated with the creation of (intergranular or transgranular) surfaces, T_0:

$$K_*(c) = K_a(c) + K_r(c) + K_\mu(c) = T_0 \tag{1}$$

This requirement can be restated by considering K_a and K_r as part of the net applied mechanical field, K_A, and $K_\mu = -T_\mu$ as part of the internal toughness, T, i.e.

$$\begin{aligned} K_A(c) &= K_a(c) + K_r(c) \\ &= T_0 + T_\mu(c) = T(c) \end{aligned} \tag{2}$$

The toughness function $T(c)$ constitutes the so-called *T*-curve, the *K*-field equivalent of the *R*-curve.

Our principal aim is to express $T_\mu(c)$ in terms of grain size and other microstructural variables.[36] The stress–separation micromechanics are assumed to be governed by thermal expansion mismatch stresses, which "clamp" the interlocking bridging grains into the matrix. (We have already noted the manifestations of such internal stresses in relation to the microcracks in Fig. 2.) As the crack walls move apart, the bridging grains debond along the constrained boundary facets and then slide out against frictional tractions at these boundaries until final "rupture" at some critical strain.[31,34] Ignoring the debond stage (which consumes relatively little energy[36]), the constitutive relation between the closure stress p and (half) crack-opening displacement u may be written[32,36]

$$p(u) = p_M(1 - u/u_\ell) \tag{3}$$

where p_M is the maximum resistance stress (at $u = 0$) and $2u_\ell$ is the wall–wall displacement at bridge–matrix disengagement (at $p = 0$). For geometrically similar microstructures, these last two quantities may be determined more explicitly in terms of the grain size ℓ:[36]

$$2u_\ell = \epsilon_\ell \ell \tag{4a}$$

$$p_M = (4\epsilon_\ell \mu \sigma_R)(1 - 1/2\alpha_d^2) \tag{4b}$$

with bridge rupture strain ϵ_ℓ, coefficient of sliding friction μ, magnitude of internal stress σ_R, and ratio of bridge-spacing to grain-size $\alpha_d = d/\ell$ all *scale-independent* parameters. Schematic plots of the constitutive relation are given for different grain sizes in Fig. 5. Note that ℓ enters the formalism exclusively through the grain pullout distance u_ℓ, and *not* through the closure stress p_M.

Now consider the evolution of a half-penny crack, radius c, through the microstructure, Fig. 6. The solution for $T_\mu(c)$ may be subdivided into three domains.[36]

(A) Small Cracks: ($c < d$), no bridge intersections. The crack is assumed to initiate in a region of local matrix tensile residual stress, assumed uniform at $+\sigma_R$, whence

$$T_\mu(c) = -\psi \sigma_R c^{1/2} \tag{5}$$

with ψ a geometry coefficient.

(B) Intermediate Cracks: ($c \geq d$, $0 \leq 2u \leq \epsilon_\ell \ell$), bridges intersected. There are two contributions in this region, $T_\mu(c) = T'_\mu(c) + T''_\mu(c)$. The first is a persistent, opening post-intersection component from the tensile stress $+\sigma_R$ in (A); a Green's function integration yields

$$T'_\mu(c) = -\psi \sigma_R c^{1/2}[1 - (1 - \alpha_d^2 \ell^2/c^2)^{1/2}] \tag{6}$$

The second is a countervailing closing component due to the bridging tractions in Eq. (3). One may use the *J*-integral to determine the corresponding crack resistance component R''_μ in terms of crack-opening displacements.[50]

$$\begin{aligned} J_\mu &= 2\int_0^{u_Z} p(u)\, du \\ &= 2p_M u_Z(1 - u_Z/\epsilon_\ell \ell) = R''_\mu(u_Z) \end{aligned} \tag{7}$$

where the displacement $u_Z = u_Z(c)$ at the edge of the bridging zone (i.e., point of first bridge intersection at $c = d = \alpha_d \ell$, Fig. 6) may be evaluated separately from the approximate

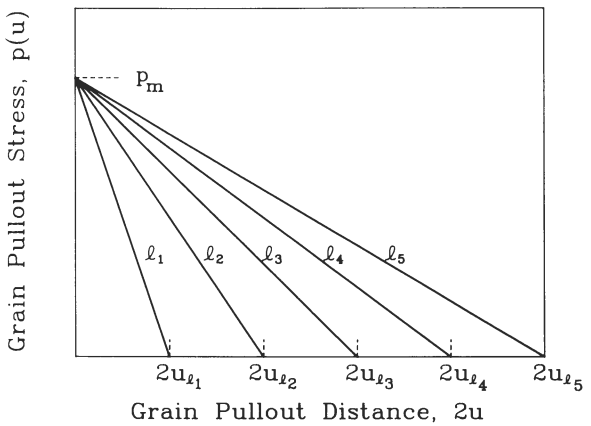

Fig. 5. Schematic plots of constitutive relation Eq. (3) for different grain sizes ($\ell_1 < \ell_2 < \ell_3 < \ell_4 < \ell_5$). Note that pullout distance u_ℓ in Eq. (4*a*) scales linearly with grain size ℓ, but that corresponding stress p_M in Eq. (4*b*) is completely *independent* of ℓ.

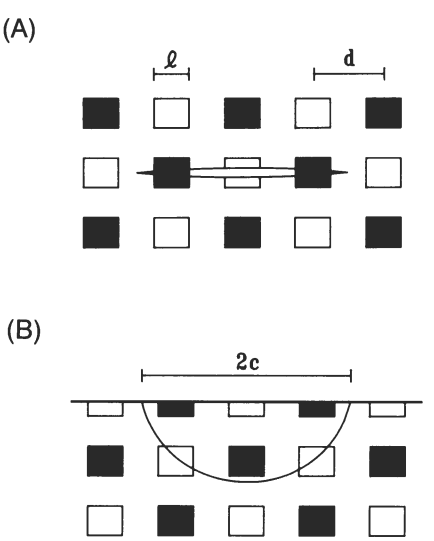

Fig. 6. Schematic of growth of pennylike crack in bridging field: (A) side view, (B) projection view. (Open squares are out-of-plane bridging grains.)

Sneddon crack profile relation

$$u_Z(c) = (\psi K_A/E')[(c^2 - \alpha_d^2\ell^2)/c]^{1/2} \quad (8)$$

to give $R''_\mu(c)$. The toughness T''_μ may be related to the crack resistance R''_μ by eliminating J_A and K_A from the equivalent equilibrium relations $J_A = T_0^2/E' + R''_\mu$ and $K_A = T_0 + T''_\mu$ (Eq. (2)) via $J_A = K_A^2/E'$:[50]

$$T''_\mu(c) = [E'R''_\mu(c)]^{1/2}\{[1 + T_0^2/E'R''_\mu(c)]^{1/2} - [T_0^2/E'R''_\mu(c)]^{1/2}\} \quad (9)$$

Equation (9) is an implicit function in T''_μ, so Eqs. (2) and (7) to (9) must be solved simultaneously.[50]

(C) Large Cracks: ($c \gg d$, $2u_Z \geq \epsilon_\ell \ell$), bridging zone translates with crack, and $T_\mu = T'_\mu + T''_\mu$ becomes invariant with crack size.

We shall consider the explicit form of $T(c)$ in specific relation to our aluminas later. For the present we simply emphasize that the contribution to the toughness from the local matrix tensile residual stress is negative (Eqs. (5) and (6)) and thereby diminishes the stability at small crack sizes, whereas the contribution from the frictional pullout is positive (Eq. (9)) and strongly enhances the stability at large crack sizes.[32,35] It is these opposite tendencies at extremes of crack size that account for the spontaneous initiation and arrest of the microcracks in Fig. 2.

(2) Flaws and Strength Characteristics

Now consider the evolution of flaws through the bridging field under the action of a uniform applied stress σ_a, corresponding to a stress-intensity factor[30,33]

$$K_a = \psi\sigma_a c^{1/2} \quad (10)$$

so that Eq. (2) transposes to

$$\sigma_a(c) = (1/\psi c^{1/2})[T(c) - K_r(c)] \quad (11)$$

The strength response may then be determined by properly applying the crack instability condition $d\sigma_a(c)/dc \geq 0$ (equivalent to $dK_A(c)/dc \geq dT(c)/dc$[48]). In relation to Griffith flaws ($T = T_0 = \text{const}$, $K_r = 0$), for which Eq. (11) reduces to a single, monotonically diminishing branch, the stabilizing influence of the $T(c)$ and $K_r(c)$ fields is manifest as maxima in the $\sigma_a(c)$ function.[33,36] Ultimate failure at $\sigma_a = \sigma_m$ corresponds to the greatest of these maxima.

It remains to specify the quantities K_r in Eq. (11) and initial sizes c_i for the flaw types of interest. For the controlled Vickers flaws used to obtain the data in Fig. 4, we have[45,51]

$$K_r = \chi P/c^{3/2} \quad (12)$$

with P the indentation load and χ an elastic–plastic contact coefficient; c_i is then determined by the condition $\sigma_a = 0$ in Eq. (11). For the grain-facet processing flaws which determine the *intrinsic* strength characteristics, we simply set $K_r = 0$. According to the observations in Section III(1), the initial size of these flaws is on the order of one grain facet but, to allow conservatively for the possibility of preexisting extended microcracks (Fig. 2), we assume one bridge spacing, $c_i = \alpha_d\ell$. Finally, for *extrinsic* flaws we again set $K_r = 0$; in this case the values of c_i are to be specified independently.

V. Analysis of Alumina Data in Terms of Bridging Model

Now let us apply the theory of the previous section to obtain fits to the data in Fig. 4 and thence to determine the T-curves for our aluminas. We do this by choosing initial values for the microstructural parameters and then adjusting these parameters using an iterative algorithm.

(1) Regression Algorithm

We begin by specifying first values for the material and geometrical parameters in the strength formulation, using estimates from a previous analysis on a commercial alumina.[36] Some of these parameters are regarded as invariants in the regression: geometry coefficient $\psi = 1.24$ (penny cracks),[‡‡] Young's modulus $E' = 409$ GPa, and indentation flaw parameter $\chi = 0.018$ ("pure" alumina).[33] Other starting parameters are treated as adjustable: $T_0 = 2.5$ MPa·m$^{1/2}$ for the grain-boundary toughness and $\sigma_R = 155$ MPa for the internal stress; bridge rupture strain $\epsilon_\ell = 0.14$ and (normalized) bridge spacing $\alpha_d = 1.5$; and friction coefficient $\mu = 1.8$.

The regression algorithm for best fitting the $\sigma_m(P)$ data is based on a matrix search routine:[33,36] (i) compute trial T-curve based on starting values of parameters; (ii) evaluate function $\sigma_a(c)$ in Eq. (11), using all individual (rather than mean) test points, at each indentation load and grain size for which experimental data are available; (iii) determine the inert strength σ_m as the largest maximum in each such $\sigma_a(c)$ function; (iii) compare predicted strengths with measured values for each set of parameters, and evaluate the net variance in σ_m over all loads and grain sizes; (iv) adjust the floating parameters ($T_0, \sigma_R, \epsilon_\ell, \alpha_d, \mu$), with increasing refinement in the increment size in successive iterations, and thence determine the parameter set with minimum variance.

(2) Data Fits and Deconvolution of T-Curves

The best fit to the strength data for our alumina corresponds to the following material parameters: $T_0 = 2.75$ MPa·m$^{1/2}$, $\sigma_R = 380$ MPa, $\epsilon_\ell = 0.040$, $\alpha_d = 1.0$, and $\mu = 1.6$; the standard deviation in σ_m over all data is 17 MPa. This parameter fit is represented by the solid curves in Fig. 4. (Compared with the above starting values from our earlier data fit, we may note an increase in T_0 and σ_R, a decrease in ϵ_ℓ.) It can be seen that the theory accounts for the major grain-size dependencies in the indentation–strength data sets, particularly the relative positions and widths of the plateaus and the crossover tendencies. For ready comparison, the curves for the various grain sizes are plotted on the composite diagram of Fig. 7.

Deconvoluted T-curves resulting from the parameter fit are shown in Fig. 8. The strongly decreasing toughness with crack extension at small crack sizes (negative branch) reflects the high level of local (thermal expansion anisotropy) tensile stress acting on the flaw. After the first bridge intersection at $c = \alpha_d\ell$ the toughness curves rise markedly (positive branch), especially for the coarser grain structures, reflecting the scaling effect in the grain pullout length. It is this rising por-

[‡‡]Strictly, ψ should be a function of the ratio of crack length to specimen thickness. In our experiments the maximum crack size at failure was ≈0.5 mm, i.e., about 20% of the specimen thickness, which leads to a maximum error of ≈7%.[52] This error is considerably smaller than the shifts in strength values from grain size to grain size in Fig. 4 and is neglected here.

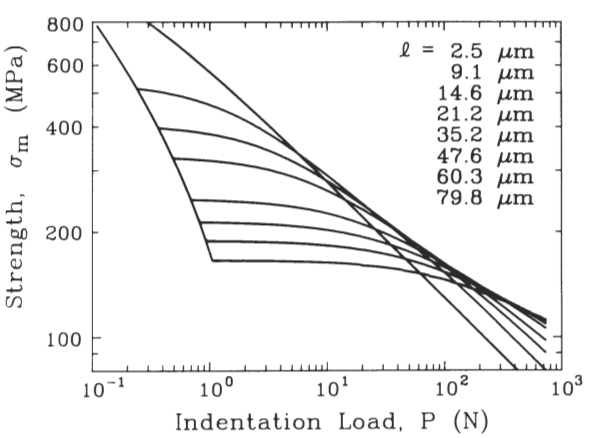

Fig. 7. Composite plot of best-fit $\sigma_m(P)$ curves for the aluminas in Fig. 4. Note tendency for curves at different grain size to cross over at intermediate indentation loads.

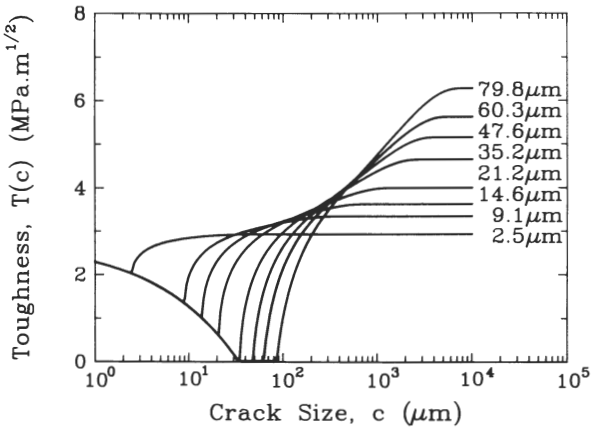

Fig. 8. Toughness curves for aluminas of grain sizes, deconvoluted from theoretical fits in Fig. 7.

tion of the curves that largely determines the strength properties. A flaw which becomes unstable at applied load $K_A = K_a = \psi\sigma_a c^{1/2}$ (Eq. (10)) on the negative branch just to the left of the minimum propagates unstably and arrests on the positive branch; this accounts for the "pop-in" behavior observed experimentally.[31] The particular curve for which the condition $c = \alpha_d \ell$ coincides with the abscissa ($K_A = T = 0$ in Eq. (2)) determines the critical grain size for *spontaneous* pop-in; from Fig. 8 we estimate $\ell \approx 30$ μm for our alumina, consistent with the first observation of microcracking in Fig. 2.

From the parameter fits in Fig. 4 we determine the strength/grain-size characteristic for *intrinsic* flaws ($K_r = 0$) shown in Fig. 9. Recall our assumption of an initial size $c_i = \alpha_d \ell$ for such flaws; in fact, the computed strength curve is insensitive to wide variations in this initial flaw size,[36] as befits a truly intrinsic property. The predicted curve has a slope close to, but not exactly, $-\frac{1}{2}$; nor, indeed, is the curve linear on the logarithmic plot. Note that only the data point corresponding to the very smallest grain size deviates significantly from this curve, suggesting that the stabilizing influence of the $T(c)$ function exerts a controlling influence in all but the finest microstructures.

VI. Discussion

The bridging model accounts for the main features of the indentation strength–load response for our aluminas. It explains, in particular, the flaw tolerance qualities apparent in the data of Fig. 4 and thereby accentuates the inadequacy of the simple Griffith flaw concept. It is no longer valid to consider toughness T as a material constant (although the intrinsic grain-boundary toughness T_0 *is* invariant) or the critical flaw size at final instability to be proportional to grain size: the stabilizing influence of the T-curve fundamentally and dramatically transforms the micromechanics of failure.

We noted the capacity of the bridging theory to fit all the major trends in the alumina indentation–strength data of Fig. 4, over the entire range of grain sizes covered. Because there are several adjustable parameters involved in this fit, the "agreement" cannot be taken as "proof" of the model.[36] The validity of the bridging concept rests with the direct observations of crack evolution reported elsewhere.[31] Once "calibrated", the formalism allows us to quantify the role of grain size (as well as other microstructural variables) in the strength characteristics. Thus we recall that the grain-size exponent in the strength curve for intrinsic flaws in Fig. 9 is close, but *not* exactly equal, to the value $-\frac{1}{2}$ for ideal Griffith flaws: there is nothing in the bridging theory to suggest that this exponent should necessarily assume any universal value or indeed that the relation should be power law at all.

In this context it is interesting to compare the fit to the present alumina data with the earlier fit to a commercial alumina.[36] There, a forced power-law fit yielded an exponent closer to $-\frac{1}{3}$. Two experimental observations distinguish our material from that used in the earlier study: the microstructure is considerably more uniform in size and shape (the commercial material showed evidence of some abnormal grain growth), and the fracture mode has a stronger transgranular component. This may be correlated with the relatively high grain-boundary toughness T_0 and internal residual stress σ_R, and low bridge rupture strain ϵ_ℓ, indicators of grain boundaries which are less susceptible to debonding, hence pullout. Here is an example where an element of control in microstructural development could be counterproductive: comparative examination of the indentation–strength data sets confirms that the present materials have less pronounced T-curves and are therefore less flaw tolerant. The implication is that inhomogeneity and nonuniformity in the microstructure, e.g., elongate grains (to increase u_ℓ in Eq. (4*a*)[36]), may actually be desirable features from the structural standpoint.

The bridging model also provides insights into the role of flaw states in the Orowan–Petch transition referred to in Section I. To illustrate, we replot from Fig. 9 the strength data for unindented surfaces as a function of inverse square root grain size in Fig. 10. Included in Fig. 10 are the corresponding predicted responses for intrinsic flaws (solid curve, $K_r = 0$, $c_i = \alpha_d \ell$) and extrinsic flaws (dashed curve, $K_r = 0$, c_i as

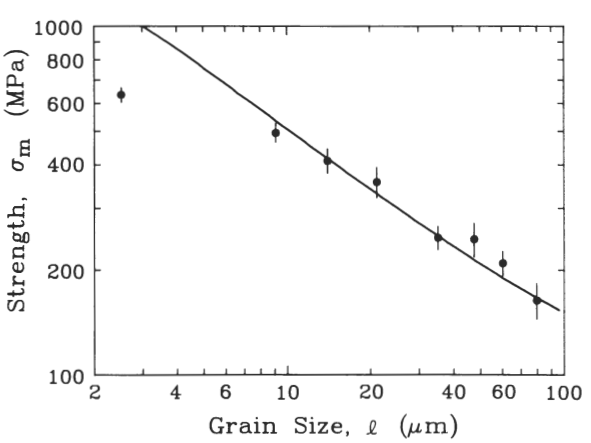

Fig. 9. Strength versus grain size for alumina. Data points are breaks from specimens without indentations; solid curve is prediction for intrinsic, microstructure-controlled flaws using indentation-strength parameters from fits in Fig. 4.

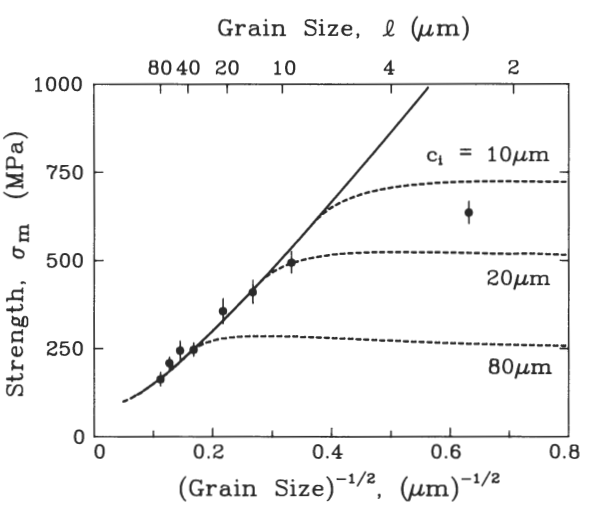

Fig. 10. Similar to Fig. 9, but with abscissa replotted as inverse square root of grain size, with data points again for unindented specimens and solid curve for intrinsic flaws. Also included as dashed curves are predictions for extrinsic flaws of specified initial size c_i. Note insensitivity of strength to flaw characteristics in large-grain-size domain.

specified). We note that the dashed and solid curves merge in the large grain-size (Orowan) domain. The insensitivity of the predictions to any assumptions concerning type or size of initial flaw in this domain (attributable to the T-curve stabilization) indicates a failure condition determined exclusively by material properties. Note again that the solid curve is not exactly linear in this region, as would obtain if true Griffith–Orowan behavior were to prevail.[§§] On the other hand, in the small-grain-size (Petch) domain the strengths are highly flaw sensitive, and the dashed curves diverge substantially from the Orowan branch, the more so as c_i increases. On passing into this region, the extrinsic flaws become increasingly larger than their microstructural counterparts and thereby traverse the upper reaches of the T-curves in Fig. 8 where precursor stable crack growth prior to failure no longer occurs.[32,48] We note that only one of the data points in Fig. 10, that at the finest grain size ($\ell = 2.5\ \mu m$), appears to fall into the extrinsic domain: this result implies an initial flaw size $c_i \approx 15\ \mu m$ for our polished surfaces. For the larger extrinsic flaws, the dashed curves in Fig. 10 pass through a slight maximum at fine grain sizes (i.e., into a region in which σ_m actually *increases* with respect to ℓ), reflecting the crossover to positive dependence of steady-state toughness on grain size at right in Fig. 8.

The results of the present study have some intriguing implications concerning microstructural design for improved structural materials. We have already alluded to the potential for engineering grain-boundary structures (as they affect T_0, σ_R, ϵ_ℓ, etc.) and grain texture (elongate grains) to impart respectable toughness properties to otherwise inherently brittle single-phase ceramics.[36] Perhaps the most far-reaching conclusion to emerge from the analysis is the relatively benign role of processing flaws in ceramics with strong T-curve behavior. The relentless elimination of every last defect, as advocated by some,[14,53–55] is not necessarily the ultimate in processing strategies.

Our study has focused on alumina, for which the mechanism of toughening is bridging grain pullout. However, we would emphasize that similar grain-size dependencies are to be expected in any material which exhibits T-curve (R-curve) behavior, e.g., whether due to incorporated second phases (e.g., fibers, whiskers), phase transformations, microcrack cloud formation, or any other subsidiary energy-dissipative process. This is not to preclude the possibility of ceramics without an R-curve, e.g., single-phase cubic ceramics, exhibiting an Orowan–Petch transition; but there the Orowan branch can no longer be defined exclusively by material properties and requires additional detailed specification of the intrinsic-flaw micromechanics.

Acknowledgments: The authors acknowledge discussions on different aspects of this work with several colleagues, including T.-J. Chuang, R. F. Cook, E. R. Fuller, Jr., Y.-W. Mai, and D. B. Marshall. We are also grateful to S. Darby for assistance with specimen preparation.

References

[1]I. B. Cutler, "Strength Properties of Sintered Alumina in Relation to Porosity and Grain Size," *J. Am. Ceram. Soc.*, **40** [1] 20–23 (1957).

[2]F. P. Knudsen, "Dependence of Mechanical Strength of Brittle Polycrystalline Specimens on Porosity and Grain Size," *J. Am. Ceram. Soc.*, **42** [8] 376–87 (1959).

[3]W. B. Crandall, D. H. Chung, and T. J. Gray, "The Mechanical Properties of Ultra-Fine Hot-Pressed Alumina"; pp. 349–76 in Mechanical Properties of Engineering Ceramics. Edited by W. W. Kriegel and H. Palmour III. Interscience Publishers, New York, 1961.

[4]R. J. Charles and R. R. Shaw, "Delayed Failure of Polycrystalline and Single-Crystal Alumina," General Electric Report No. 62-RL-3081 M, 1962.

[5]R. M. Spriggs and T. Vasilos, "Effect of Grain Size on Transverse Bend Strength of Alumina and Magnesia," *J. Am. Ceram. Soc.*, **46** [5] 224–28 (1963).

[6]R. M. Spriggs, J. B. Mitchell, and T. Vasilos, "Mechanical Properties of Pure, Dense Aluminum Oxide as a Function of Temperature and Grain Size," *J. Am. Ceram. Soc.*, **47** [7] 323–27 (1964).

[7]E. M. Passmore, R. M. Spriggs, and T. Vasilos, "Strength–Grain Size–Porosity Relations in Alumina," *J. Am. Ceram. Soc.*, **48** [1] 1–7 (1965).

[8]D. B. Binns and P. Popper, "Mechanical Properties of Some Commercial Alumina Ceramics," *Proc. Br. Ceram. Soc.*, **6**, 71–82 (1966).

[9]S. C. Carniglia, "Reexamination of Experimental Strength-vs-Grain Size Data for Ceramics," *J. Am. Ceram. Soc.*, **55** [5] 243–49 (1972).

[10]R. W. Rice, "Strength/Grain Size Effects in Ceramics," *Proc. Br. Ceram. Soc.*, **20**, 205–57 (1972).

[11]A. G. Evans and G. Tappin, "Effects of Microstructure on the Stress to Propagate Inherent Flaws," *Proc. Br. Ceram. Soc.*, **20**, 275–97 (1972).

[12]R. E. Tressler, R. A. Langensiepen, and R. C. Bradt, "Surface-Finish Effects on Strength vs Grain Size Relations in Polycrystalline Al_2O_3," *J. Am. Ceram. Soc.*, **57** [5] 226–27 (1974).

[13]E. Dörre and H. Hübner, Alumina: Processing, Properties and Applications; Ch. 3. Springer-Verlag, New York, 1984.

[14]N. McN. Alford, K. Kendall, and J. D. Birchall, "Strength/Microstructure Relation in Al_2O_3 and TiO_2," *Adv. Ceram. Mater.*, **3** [2] 113–17 (1988).

[15]E. Orowan, "Fracture and Strength of Solids," *Rep. Prog. Phys.*, **12**, 186–232 (1948).

[16]N. J. Petch, "Cleavage Strength of Polycrystals," *J. Iron Steel Inst., London*, **174** [1] 25–28 (1953).

[17]R. W. Rice, S. W. Freiman, R. C. Pohanka, J. J. Mecholsky, Jr., and C. C. Wu, "Microstructural Dependence of Fracture Mechanics Parameters in Ceramics"; pp. 849–76 in Fracture Mechanics of Ceramics, Vol. 4. Edited by R. C. Bradt, D. P. H. Hasselman, and F. F. Lange. Plenum Press, New York, 1978.

[18]R. W. Rice, S. W. Freiman, and J. J. Mecholsky, "Dependence of Strength-Controlling Fracture Energy on the Flaw Size to Grain Size Ratio," *J. Am. Ceram. Soc.*, **63** [3–4] 129–36 (1980).

[19]V. D. Krstic, "Grain-Size Dependence of Fracture Stress in Anisotropic Brittle Solids," *J. Mater. Sci.*, **23** [1] 259–66 (1988).

[20]J. P. Singh, A. V. Virkar, D. K. Shetty, and R. S. Gordon, "Strength–Grain Size Relations in Polycrystalline Ceramics," *J. Am. Ceram. Soc.*, **62** [3–4] 179–83 (1979).

[21]A. G. Evans, "Dimensional Analysis of the Grain-Size Dependence of Strength," *J. Am. Ceram. Soc.*, **63** [1–2] 115–16 (1980).

[22]A. V. Virkar, D. K. Shetty, and A. G. Evans, "Grain-Size Dependence of Strength," *J. Am. Ceram. Soc.*, **64** [3] C-56–C-57 (1981).

[23]R. W. Rice and D. Lewis, "Limitations and Challenges in Applying Fracture Mechanics to Ceramics"; pp. 659–76 in Fracture Mechanics of Ceramics, Vol. 5. Edited by R. C. Bradt, A. G. Evans, D. P. H. Hasselman, and F. F. Lange. Plenum Press, New York, 1983.

[24]H. Hübner and W. Jillek, "Sub-Critical Crack Extension and Crack Resistance in Polycrystalline Alumina," *J. Mater. Sci.*, **12** [1] 117–25 (1977).

[25]R. Knehans and R. W. Steinbrech, "Memory Effect of Crack Resistance During Slow Crack Growth in Notched Al_2O_3 Bend Specimens," *J. Mater. Sci. Lett.*, **1** [8] 327–29 (1982).

[26]R. W. Steinbrech, R. Knehans, and W. Schaarwächter, "Increase of Crack Resistance During Slow Crack Growth in Al_2O_3 Bend Specimens," *J. Mater. Sci.*, **18** [10] 265–70 (1983).

[27]R. Knehans and R. W. Steinbrech, "Effect of Grain Size on the Crack Resistance Curves of Al_2O_3 Bend Specimens"; pp. 613–19 in Science of Ceramics, Vol. 12. Edited by P. Vincenzini. Ceramurgia, Imola, Italy, 1984.

[28]M. V. Swain, "R-Curve Behavior in a Polycrystalline Alumina Material," *J. Mater. Sci. Lett.*, **5** [12] 1313–15 (1986).

[29]R. W. Steinbrech and O. Schmenkel, "Crack-Resistance Curves of Surface Cracks in Alumina," *J. Am. Ceram. Soc.*, **71** [5] C-271–C-273 (1988).

[30]R. F. Cook, B. R. Lawn, and C. J. Fairbanks, "Microstructure–Strength Properties in Ceramics: I, Effect of Crack Size on Toughness," *J. Am. Ceram. Soc.*, **68** [11] 604 (1985).

[31]P. L. Swanson, C. J. Fairbanks, B. R. Lawn, Y.-W. Mai, and B. J. Hockey, "Crack-Interface Grain Bridging as a Fracture Resistance Mechanism in Ceramics: I, Experimental Study on Alumina," *J. Am. Ceram. Soc.*, **70** [4] 279–89 (1987).

[32]Y.-W. Mai and B. R. Lawn, "Crack-Interface Grain Bridging as a Fracture Resistance Mechanism in Ceramics: II, Theoretical Fracture Mechanics Model," *J. Am. Ceram. Soc.*, **70** [4] 289–94 (1987).

[33]R. F. Cook, C. J. Fairbanks, B. R. Lawn, and Y.-W. Mai, "Crack Resistance by Interfacial Bridging: Its Role in Determining Strength Characteristics," *J. Mater. Res.*, **2** [3] 345–56 (1987).

[34]P. L. Swanson, "Crack-Interface Traction: A Fracture-Resistance Mechanism in Brittle Polycrystals"; pp. 135–55 in Advances in Ceramics, Vol. 22, Fractography of Glasses and Ceramics. American Ceramic Society, Columbus, OH, 1988.

[35]S. J. Bennison and B. R. Lawn, "Flaw Tolerance in Ceramics with Rising Crack-Resistance Characteristics," *J. Mater. Sci.*, **24** [9] 3169–75 (1989).

[36]S. J. Bennison and B. R. Lawn, "Role of Interfacial Grain-Bridging Sliding Friction in the Crack-Resistance and Strength Properties of Nontransforming Ceramics," *Acta Metall.*, **37** [10] 2659–71 (1989).

[37]R. L. Coble, "Sintering of Crystalline Solids—II. Experimental Test of Diffusion Models in Porous Compacts," *J. Appl. Phys.*, **32** [5] 793–99 (1961).

[38]S. J. Bennison and M. P. Harmer, "A History of the Role of MgO in the Sintering of α-Al_2O_3," *Ceramic Transactions*, Vol. 7, Sintering of Advanced Ceramics. Edited by C. A. Handwerker, J. E. Blendell, and W. A. Kaysser.

[§§]At very large grain sizes the strength is actually predicted to fall to zero, corresponding to unlimited unstable extension of the intrinsic flaws. Material compacts with microstructures on this scale will tend to fail spontaneously on cooling from the processing temperature.

American Ceramic Society, Westerville, OH, 1989.

[39]S. K. Roy and R. L. Coble, "Solubilities of Magnesia, Titania, and Magnesium Titanate in Aluminum Oxide," *J. Am. Ceram. Soc.*, **5** [1] 1–6 (1968).

[40]E. C. M. Pennings and W. Grellner, "Precise Nondestructive Determination of the Density of Porous Ceramics," *J. Am. Ceram. Soc.*, **72** [2] 1268–70 (1989).

[41]J. C. Wurst and J. A. Nelson, "Lineal Intercept Technique for Measuring Grain Size in Two-Phase Polycrystalline Ceramics," *J. Am. Ceram. Soc.*, **55** [2] 109 (1972).

[42]D. B. Marshall, "An Improved Biaxial Flexure Test for Ceramics," *Am. Ceram. Soc. Bull.*, **59** [5] 551–53 (1980).

[43]M. Hillert, "Theory of Normal and Abnormal Grain Growth," *Acta Metall.*, **13** [3] 227–38 (1965).

[44]C. A. Bateman, S. J. Bennison, and M. P. Harmer, "Mechanism for the Role of Magnesia in the Sintering of Alumina Containing Small Amounts of a Liquid Phase," *J. Am. Ceram. Soc.*, **72** [7] 1241–44 (1989).

[45]D. B. Marshall and B. R. Lawn, "Residual Stress Effects in Sharp-Contact Cracking: I. Indentation Fracture Mechanics," *J. Mater. Sci.*, **14** [9] 2001–12 (1979).

[46]D. B. Marshall, B. R. Lawn, and P. Chantikul, "Residual Stress Effects in Sharp-Contact Cracking: II. Strength Degradation," *J. Mater. Sci.*, **14** [9] 2225 (1979).

[47]B. R. Lawn, "The Indentation Crack as a Model Indentation Flaw"; pp. 1–25 in Fracture Mechanics of Ceramics, Vol. 5. Edited by R. C. Bradt, A. G. Evans, D. P. H. Hasselman, and F. F. Lange. Plenum Press, New York, 1983.

[48]Y.-W. Mai and B. R. Lawn, "Crack Stability and Toughness Characteristics in Brittle Materials," *Annu. Rev. Mater. Sci.*, **16**, 415–39 (1986).

[49]B. R. Lawn and T. R. Wilshaw, Fracture of Brittle Solids; Ch. 3. Cambridge University Press, London, U.K., 1975.

[50]R. F. Cook, "Transient Fracture Resistance in the Weak Toughening Limit"; pp. 2747–55, in Advances in Fracture Research, I.C.F. 7. Edited by K. Salama, R. Ravi-Chandra, D. M. R. Taplin, and P. Rama-Rao. Pergamon Press, New York, 1989.

[51]B. R. Lawn, A. G. Evans, and D. B. Marshall, "Elastic/Plastic Indentation Damage in Ceramics: The Median/Radial Crack System," *J. Am. Ceram. Soc.*, **63** [9–10] 574–81 (1980).

[52]J. C. Newman, Jr., and I. S. Raju, "An Empirical Stress-Intensity Factor Equation for the Surface Crack," *Eng. Fract. Mech.*, **15**, 185–92 (1981).

[53]F. F. Lange, "Processing-Related Fracture Origins: I, Observations in Sintered and Isostatically Hot-Pressed Al_2O_3/ZrO_2 Composites," *J. Am. Ceram. Soc.*, **66** [6] 396–98 (1983).

[54]F. F. Lange and M. Metcalf, "Processing-Related Fracture Origins: II, Agglomerate Motion and Cracklike Internal Surface Caused by Differential Sintering," *J. Am. Ceram. Soc.*, **66** [6] 398–406 (1983).

[55]F. F. Lange, B. I. Davies, and I. A. Aksay, "Processing-Related Fracture Origins: III, Differential Sintering of ZrO_2 Agglomerates in Al_2O_3/ZrO_2 Composite," *J. Am. Ceram. Soc.*, **66** [6] 407 (1983). □